RSC Advances

Crystal orientation dependence of crack growth and stress evolution in single crystal nickel: a molecular dynamics simulation-based cohesive zone model

Yuan Qi[1], Wen-Ping Wu[1, 2]*, Yun-Bing Chen[1], Ming-Xiang Chen[1, 2]

[1]*Department of Engineering mechanics, School of Civil Engineering, Wuhan University, Wuhan, China*
[2]*State Key Laboratory of Water Resources & Hydropower Engineering Science, Wuhan University, Wuhan,*

China

Abstract

The crack growth and stress evolution of single crystal nickel under three different crystal orientations ($X[100]$, $Y[010]$, $Z[001]$; $X[110]$, $Y[\bar{1}10]$, $Z[001]$; $X[111]$, $Y[\bar{1}10]$, $Z[\bar{1}\bar{1}2]$) were studied by introducing a cohesive zone model (CZM) based on molecular dynamics (MD) simulation. The results indicated that different crystal orientations have significant effect on the fracture mechanisms and stress distribution characteristics. Under the $X[100]$, $Y[010]$, $Z[001]$ orientation, void nucleation and growth was observed during the crack propagation; Under the $X[110]$, $Y[\bar{1}10]$, $Z[001]$ orientation, atomic configurations basically remained unchanged throughout the crack growth, which represented a brittle process; Dissimilarly, blunting and slip bands occurred at the front of crack tip for the $X[111]$, $Y[\bar{1}10]$, $Z[\bar{1}\bar{1}2]$ orientation. These different mechanisms resulted in different stress distributions along the crack path and crack growth rates. Moreover, based on the calculation of the CZM, the relationship between stress and opening displacement was obtained, which provided useful information for understanding the crystal orientation dependent on the atomic-scale fracture mechanisms and associated mechanical properties.

---

* Corresponding author. Tel: +86-27-68775496; Fax: +86-27-68775496
 E-mail: wpwu@whu.edu.cn

Key Words

Molecular dynamics simulation, crystal orientation, cohesive zone model, crack growth, single crystal nickel

1. Introduction

Fracture is a universal and complex problem which spans many disciplines in the physical sciences and engineering. Classical theory of continuum fracture and some empirical formulas at macroscopic are well established and utilized [1-4]. Yet, in atomic scale, the crack growth is in fact a progressive process of material degeneration, and the geometry feature of the crack tip would cause non-physical stress singularity. Macroscopic fracture mechanical theories based on phenomenological hypotheses, hereby, are no longer sufficient and even improper to resolve the very essence of the physical mechanisms. Hence, more micro-level investigations are naturally demanded.

Molecular dynamics (MD) simulation have been proven to be a useful tool for its modeling atomic scale failure process and analyzing stress evolution around the crack tip from an atomistic standpoint [5-7]. Recently, many fracture events have been carried out by utilizing the molecular dynamic simulations, which includes dynamic fracture instability [8, 9], strain rate, size and temperature dependency on crack propagation [10-13], microstructure and stress field near crack tip[14-16], brittle and ductile behaviors[12, 17-19], intergranular and transgranular crack propagation behavior [20], etc. One of the critical elements that influence fracture behavior and metal strength is the lattice orientation. Zhang and Ghosh [15] investigated the interaction of dislocation networks and twins and their variances in different crystal orientations on atomic level. Abraham and

Broughton [17] studied the cleavage direction by setting three different pre-crack orientations, and indicated that atomic stress rather than surface energy controls brittle crack growth. Xie *et al.* [21] fabricated three cracks and studied the influence of crystal orientation of twin formation from crack tip. Mei *et al.* [22] studied the surface energy and slip planes in rare metal tantalum (Ta) with different crack orientations, and proposed a new criterion to distinguish brittle from ductile fracture. These studies indicated that the crystal orientations have an important effect on the microstructure evolution and failure mechanisms of materials.

Due to material failure can be determined by the stresses and strains of strength theory, related research has indicated that atomic stress played a controlling role in nanoscale fracture, it is essential to consider the stress state during crack growth [7, 17]. However, when considering the stress singularity at crack-tip, it was inappropriate to calculate directly the stress state near the crack-tip. The cohesive zone model (CZM), as a method for calculation of local properties in the field of fracture mechanics, has been extensively used because it avoided the stress singularity at the crack-tip and represented the physics of the fracture process at the atomic scale [23-25]. Especially, the CZM can adequately track crack propagation dynamics and obtain the constitutive behavior (traction-displacement relationship) of the fracture, which was not obtained only by MD simulation [26, 27]. Therefore, it was effective and of interesting to apply a MD-based CZM for analyzing the influence of crystal orientation on the stress state and microstructure evolution near the crack-tip and the associated fracture mechanisms.

In this study, the crack-tip stress distribution and fracture mechanisms were investigated using a MD-based CZM in a pre-crack single crystal nickel with different orientations. The objective of the present work is to reveal the influence of crystal orientation on the crack propagation and fracture mechanisms. Meanwhile, based on the calculation of CZM, the

relationship between crack-tip stress field and microstructure evolution, stress and opening displacement as the crack propagates were determined from an atomic physics standpoint.

2. Modeling and simulation

2.1. Model geometry and simulation process

In this paper, MD-based CZM are performed to study the influence of the orientation on the crack propagation and fracture mechanisms in a pre-crack single crystal nickel. The geometry of the system of the crack propagation is shown in Fig. 1a. A pre-crack with 1/10 of the size of the *X*-**dimension** is inserted on the left edge of the sample along the *X* direction by removing atoms. That is, the size of *X*-dimension is much larger than the crack length so that the edge effects are eliminated for most of the crack growth of interest. The sample dimension in the *X*-axis is chosen to be sufficiently long so that steady-state crack propagation is obtained during MD simulations and the right side of the crystal is fixed for motions in *X* -direction to limit boundary effects. The top and bottom 2-layer atoms, which have a thickness of potential cut-off distance, are fixed. Periodic boundary conditions are formulated in the Z direction, and non-periodic boundary conditions are applied in the *X* and *Y* directions. To study the crystal orientation effect, the samples with three different orientations (*X*[100], *Y*[010], *Z* [001]; *X*[110], *Y*[$\bar{1}$10], *Z*[001]; *X*[111], *Y*[$\bar{1}$10], *Z*[$\bar{1}\bar{1}$2]) are set up as shown in Tab.1, and the initial crack fronts of these three samples with different orientations are along the [100], [110], [111] direction, respectively. In the present MD simulations, the embedded-atom-method (EAM) potential provided by Mishin *et al.* [28] is adopted, which has previously been successfully applied to simulate the failure process of face-centered cubic (FCC) single crystal nickel [10,11,14, 27, 29].

To accurately and quantitatively predict the crack propagation and failure properties of microstructures, the local nanoscale properties were considered. Fig. 1b shows the schematic of regions used to calculate the local properties using CZM. The initial configuration is divided into n = 50 cells (where the width of one cell is the lattice constant of nickel), the height of the cohesive zone is 4 cells (four times the lattice constant of nickel) as shown in Fig. 1b. That is for calculating the crack opening displacement and establishing the relationship governing their cohesive behavior from discrete atomistic simulations.

At the beginning of the simulation, the system is relaxed using the conjugate gradient method to reach a minimum thermo-energy state. Then the models are stretched in the Y direction by an incrementally displacement loading every 20 ps and the global strain rate of $1.0\times10^8 s^{-1}$. In the next step, the same displacement increment was applied again, and the process was repeated. Finally, the deformed configuration of the system was computed by MD simulations, where the simulation was carried out by integrating Newton's equations of motion for all the atoms using a time step of 1×10^{-15} s. The open-source MD code LAMMPS[30] and the visualization tools AtomEye [31] were used in the atomistic simulations. As the temperature plays a critical role in crack propagation velocities of the atoms are rescaled to avoid thermal activation and the temperature is maintained at 1×10^{-4}K (approximately 0K) throughout the simulation.

2.2 Definition of stress and centro-symmetry parameter

To examine the different orientations of crack propagation at nanoscale level, the atomistic level stress tensor is recorded and studied. In this paper, we employ the stress definition, the measurement of the inter-atomic interactions between atom and its neighbors, proposed by Born and Huang [32]

$$\sigma_{\alpha\beta}(i) = -\frac{1}{2\Omega_i}\sum_{j\neq i}^{N} f_\alpha(i,j)r_\beta(i,j) \tag{1}$$

where N is the number of atoms within the cutoff-distance region around atom i, Ω_i is the volume of atom i, $f_\alpha(i,j)$ is the interactive force component by atom j on atom i, and $r_\beta(i,j)$ stands the relative position from atom j to atom i. Usually, the stress of atom i is taken as an average of atom stress within its cutoff-distance region, the average atomic stress tensor $\bar{\sigma}_{\alpha\beta}(i)$ at atom i is given by [33]

$$\bar{\sigma}_{\alpha\beta}(i) = \frac{1}{N}\sum_{j=1}^{N} \sigma_{\alpha\beta}(j) \tag{2}$$

To measure the local lattice disorder around an atom and to characterize whether the atom is part of a perfect lattice, the Centro-symmetry parameter for a single atom is defined as [34]

$$CSP = \sum_{i=1}^{6} \left|\vec{R}_i + \vec{R}_{i+6}\right|^2 \tag{3}$$

where $\vec{R}_i$ and $\vec{R}_{i+6}$ are the vectors from the central atom to the six pair of nearest neighbors in the FCC lattice. By definition, it is clearly that if the perfect FCC material is subjected to homogeneous elastic deformation, e.g. no flaws or strain localization, the value of CSP should be zero.

3. Simulation results and discussion

Three pre-cracked samples with different orientations of ($X[100]$, $Y[010]$, $Z[001]$; $X[110]$, $Y[\bar{1}10]$, $Z[001]$; $X[111]$, $Y[\bar{1}10]$, $Z[\bar{1}\bar{1}2]$) are carried out to discuss the influence of crystal orientation on crack propagation and fracture mechanisms. Detailed results of crack growth

6

process, stress field and the microstructure evolution are illustrated and analyzed in the following sections.

3.1. *X[100], Y[010], Z [001] crystal orientation*

Fig.2. shows the stress and microstructure evolutions near the crack tip during crack growth in the *X[100], Y[010], Z [001]* orientation. At a loading time of t = 300 ps, the crack does not initiate and holds in the original shape, but the stress concentration occurs at the crack tip due to the geometry singularity as shown in Fig.2a (the contour plot stands for the atomic tensile stress variation at different sites). At t=376 ps, the site of peak stress site shifts ahead along the direction of the crack tip and dislocation emits at this place (see Fig.2b). As the loading continues, at t = 386 ps and 400ps, a void is formed at the region of the dislocation nucleation, and then the void coalesced and growth to form a new crack tip at a short distance in front of the original crack with the application of loading. Meanwhile, the site of the stress concentrations move to the new crack tip of a growing crack, as shown in Figs. 2c and 2d. Subsequently, the new crack begins to grow with the highest stress at the crack tip, at t = 400 ps, the new crack linked-up with the original crack to create a longer crack along the crack path until the sample wholly fracture (Fig. 2e).

Fig. 3 quantitatively shows the atomic tensile stress as a function of the atom position along the crack path at different loading time. It can be seen that the peak tensile stress maintains about 22GPa with its site moves forward in the whole crack propagation process. At t=300ps, the peak tensile stress occurs at the crack tip, and the stress is monotonic to the atom position along the crack path at crack front. Subsequently, at t=376ps and t=386ps, dislocation emission and void formation lead to the redistribution of the atomic tensile stress and make the stress variation non-

monotonically along the crack path. Once the void link-up with the original crack, the peak tensile stress returns to the crack tip again, and the crack propagates forward in a brittle way.

3.2. *X[110], Y[$\bar{1}$10], Z[001] crystal orientation*

Fig.4. shows a detailed observation on the stress field around the crack tip and microstructure evolution during crack growth in the X [110], Y [$\bar{1}$10], Z [001] orientation. At the loading time of t= 150ps, the atomic tensile stress concentrates at the crack tip due to geometric discontinuity; these atoms at the crack tip hold their initial atomic configuration without inducing the change of microstructure, as shown in Fig.4a. At the onset of crack growth (t=190ps), a new minor crack initiates at the upper corner of the original pre-crack, and the site of stress concentration moves to the new formed crack tip. Besides, there is still no other change of the crack-tip microstructure (see Fig.4b). After crack growth initiation, the crack extends quickly and approaches fracture at t=358ps, the atomic tensile stress concentration always occurs at the crack-tip of a growing crack, as observed in Fig.4c and d. The four snapshots of crack propagation in Fig. 4 show a clean brittle fracture, the atomic configuration clearly displays almost perfectly flat atomic surfaces without inducing the change of microstructure.

To more quantitative understanding the atomic stress distribution during the process of crack propagation, the atomic tensile stress as a function of the atom position along the crack path is plotted in Fig.5. The highest tensile stress always occurs at the crack-tip of a growing crack during the whole fracture process. Meanwhile, the stress distributions are basically monotonic to the atom position along crack path at crack front due to there is no microstructure changing near the crack-tip during the process of crack propagation. Furthermore, it is obvious

that the atomic tensile stress increases slowly (from about 17 GPa increases to 20 GPa) as the crack propagates forward due to the reduction of the effective surface area.

3.3. $X[111]$, $Y[\bar{1}10]$, $Z[\bar{1}\bar{1}2]$ *crystal orientation*

Fig.6 shows the stress field and related microstructure evolution around the crack tip in the X [111], Y [$\bar{1}$10], Z [$\bar{1}\bar{1}$2] **crystal orientation**. As discussed in the former two different orientations of samples, at the early loading time (t=200ps), the atoms at the crack tip hold their initial atomic configuration, and these crack tip atoms have the highest atomic tensile stress levels, see the contour plots of the atomic tensile stress field in Fig.6a. As loading continues, crack tip blunting occurs due to the [$\bar{1}$10] dislocation emission at the loading time of t=232ps. In this case, the original atomic configuration begins to change. The analysis of the microstructure shows the dislocation emits at certain distance ahead of the crack tip where the crack tip blunts. Simultaneously, the microstructure evolution induces the change of the atomic tensile stress field around the crack tip, as shown in Fig.6b. At t=300ps, another dislocation emits from the crack tip along the [021] direction and the atoms have very high stress values at the region of dislocation is shown in Fig.6c. When these stresses are increased by stress concentrations resulting from the surface irregularities, the material reaches its yield strength in the localized region which initiates slip. As can be seen in Fig. 6d, slip bands generates and a rather large region of plastic deformation occurs in front of the growing crack. Those can be observed through a one-to-one relationship between the stress distributions and microstructure characteristics around the crack tip at t=330ps. In the next loading time of t=350ps, the slip bands and the plastic deformation zone gradually expands until the rest of the sample occupied (see Fig.6e).

Fig.7 shows the atomic tensile stress sample as a function of atom position along the crack path at different loading time for the X [111], Y [$\bar{1}$10], Z [$\bar{1}\bar{1}$2] **crystal orientation**. As observed in Fig.7, the peak tensile stress (14 GPa) occurs at the crack tip on account of geometry singularity at beginning of loading time of t=200ps, and the tensile stress field along the crack line is basically monotonic at the crack front. After the loading time of t=232ps, the tensile stress field varies non – monotonically along crack path, it goes down first, and then gradually climbs up. When the loading time t=350ps, the atoms at the just right side of the sample gets the tensile stress value equivalently to the stress of the crack tip and even surpass a bit. It suggests that the high stress value not only occurs at the crack tip but also at the region of the existence of slip bands. That is, atoms have the highest tensile stress values both at the new crack tip and at the region of plastic deformation.

4. Crack propagation dynamics for samples with three different orientations

Crack propagation dynamics is an important aspect for understanding the crack propagation and fracture behavior. In order to show quantitatively how the crystal orientations effect on the crack resistance and crack propagation dynamics, based on the calculation of the CZM, the results for the crack length as a function of loading time for three different orientations are plotted as Fig. 8(a). It can be seen that the crack propagation is susceptible to the crystal orientations and show disparate behaviors. In the X [100], Y [010], Z [001] crystal orientation, the crack does not propagate until around 355ps, then the material experiences a ductile to brittle transition, after t=375 ps, the crack grows forward quickly with an average speed of 396 m·s^{-1} until the sample final fracture. In the X [110], Y [$\bar{1}$10], Z [001] crystal orientation, the crack does not propagate until around 180ps, then the crack extends quickly from the original crack to the

final fracture with an average speed of 285 m·s^{-1}. The whole procedure is just like a brittle

fracture process. For the X [111], Y [$\bar{1}$10], Z [$\bar{1}\bar{1}$2] crystal orientation, compared with X [100], Y

[010], Z [001] and X [110], Y [$\bar{1}$10], Z [001] crystal orientations, the crack extension displays a

distinctly slow due to the formation of slip bands in front of the crack tip during the crack

propagation. The crack length almost remain the initial length at the most of run time and

eventually increase less than 18 Å until the end of run time t=500ps, the inset in Fig. 8 provide a

more detailed view of the crack extension levels as the loading time increase. The results indicate

that the crack length is closely related to the micro-structural evolution around the crack tip of

samples with different orientations.

Fig.8 (b) shows the averaged atomic tensile stress vs. the opening displacement. The

stress and opening displacement relations of the samples with different orientations under Mode

I loading are extracted from the atomic forces and motions of the cohesive zone model. Both the

samples with X [100], Y [010], Z [001] and X [110], Y [$\bar{1}$10], Z [001] orientations had their

highest tensile stress at about 1.5 Å of opening displacement. The highest averaged tensile stress

is about 18 GPa in the X [100], Y [010], Z [001] orientation, and the stress has maintained a very

high value until the opening displacement reached 2.0 Å due to the void nucleation during the

crack propagation. While in the X [110], Y [$\bar{1}$10], Z [001] orientation, the highest averaged tensile

stress is about 13 GPa, then the stress decreased quickly after reaching its maximum value at

about 1.5 Å of opening displacement. For the X [111], Y [$\bar{1}$10], Z [$\bar{1}\bar{1}$2] orientation, the averaged

tensile stress has always kept very high value due to a larger number of slip bands generation

during the crack propagation. The results indicate that the different micro-mechanisms that occur

during the processes of crack growth affect significantly opening crack and stress states.

5. Conclusions

In this paper, Molecular dynamics simulations based on the cohesive zone model have been performed to investigate the effect of crystal orientation on the crack-tip stress and crack propagation in single crystal nickel. The results indicated that crack-tip stress and microstructure evolutions depend on crystal orientations. in the X [100], Y [010], Z [001] orientation, void nucleation and growth was observed during the crack propagation, and associated with a mutation of stress at the region of void nucleation; In the X [110], Y [$\bar{1}$10], Z [001] orientation, atomic configurations near the crack tip basically remained unchanged and stress concentration always occurred at the crack tip of a growing crack throughout the crack growth, which represented a brittle process; However, crack tip blunting and slip bands occurred in the X [111], Y [$\bar{1}$10], Z [$\bar{1}\bar{1}$2] orientation, the highest stress occurred at the region of crack tip blunting and slip bands. Moreover, based on the calculation of CZM, there were obvious differences in the crack growth rate and crack opening displacement for the samples with three different orientations, respectively, which were closely related to the different fracture mechanisms caused by crystal orientation. These results provided useful information for understanding the crystal orientation dependent on the atomic-scale fracture mechanisms and stress distribution characterizes.

Acknowledgments

RSC Advances Accepted Manuscript

Reference

[1] A. A. Griffith, *Philos. T. R. SOC. A*, 1921, **221**, 163.

[2] G. R. Irwin, *J Appl Mech.*, 1957, **24**, 361.

[3] S. Y. Yarema, *Mater. Science*, 1996, **31**, 617.

[4] J. R. Rice, *J. Appli. Mech.*, 1986, **35**, 379.

[5] K. Nishimura, N. Miyazaki, *CMES: Comp. Model. Eng.*, 2001, **2**, 143.

[6] K. S. Cheung, S. Yip, *Modelling Simul. Mater. Sci. Eng.*, 1994, **2**, 865.

[7] S. Xu, X. Deng, *Nanotechnol.*, 2008, **19**, 115705.

[8] D. Holland, M. Marder, *Phys. Rev. Lett.*, 1998, **80**, 746.

[9] D. Holland, M. Marder, *Adv. Mater.*, 1999, **11**, 793.

[10] W. P. Wu, Z. Z. Yao, *Strength Mater.,* 2014, **46**, 164.

[11] W. P. Wu, Z. Z. Yao, *CMES: Comp. Model. Eng.*, 2013, **93**, 235.

[12] Y. Furuya, H. Noguchi, S. Schmauder, *Int. J. Fract.*, 2001, **107**, 139.

[13] M. F. Horstemeyer, M. I. Baskes, S. J. Plimpton, *Acta Mater.*, 2001, **49**, 4363.

[14] W. P. Wu, Z. Z. Yao, *Theor. Appli. Fract. Mech.,*2012, **62**, 67.

[15] J. Zhang, S. Ghosh, *J. Mech. Phys. Solids*, 2013, **61**, 1670.

[16] Y. Cheng, M. X. Shi, Y. W. Zhang, *Int. J. Solids Struct.*, 2012, **49**, 3345.

[17] F. F. Abraham, J. Q. Broughton, *Comput. Mater. Sci.*, 1998, **10**, 1.

[18] Y. F. Guo, C. Y. Wang, D. L. Zhao, *Mater. Sci. Eng. A*, 2003, **349**, 29.

[19] O. Nejadseyfi, A. Shokuhfar, *J. Comput. Theor. Nanoscience*, 2014, **11**, 2199.

[20] J. G.Yu, Q. X. Zhang, R. Liu, Z. F. Yue, M. K. Tang, X. W. Li, *RSC Advances*. 2014, **4**, 32749.

[21] H. Xie, T. Yu, F. Yin, C. Tang, *Mater. Sci. Eng. A*, 2013, **580**, 99.

[22] J. Mei, Y. Ni, J. Li, *Int. J. Solids Struct.*, 2011, **48**, 3054.

[23] V. Yamakov, E. Saether, D. R. Phillips, E. H. Glaessgen, *J. Mech. Phys. Solids*, 2006, **54**, 1899.

[24] C. R. Dandekar, Y. C. Shin, *Composites Part A*, 2011, **42**, 355.

[25] X. W. Zhou, J. A. Zimmerman, E. D. Reedy Jr., N. R. Moody, *Mech. Mater.*, 2008, **40**, 832.

[26] K. Park, G. H. Paulino, *Appli. Mech. Rev.*, 2011, **64**, 060802.

[27] Y. L. Li, W. P. Wu, N. L. Li, Y. Qi, *Comput. Mater. Sci.*, 2015, **104**, 212.

[28] Y. Mishin, D. Farkas, M. J. Mehl, D. A. Papaconstantopoulos, *Phys. Rev. B*, 1999, **59**, 3393.

[29] M. Karimi, T. Roarty, T. Kaplan, *Modelling Simul. Mater. Sci. Eng.*, 2006, **14**, 1409.

[30] S. J. Plimpton, *J. Comput. Phys.*, 1995, **117**, 1. < http://lammps.sandia.gov/>.

[31] J. Li, *Model. Simul. Mater. Sci. Eng.*, 2003, **11**, 173.

[32] M. Born, K. Huang, Dynamical theory of crystal lattices. 1954, *Oxford: Clarendon*.

[33] M. F. Horstemeyer, M. I. Baskes, *J. Eng. Mater. Technol.*, 1999, **121**, 114.

[34] C. L. Kelchner, S. J. Plimpton, J. C. Hamilton, *Phys. Rev. B*, 1998, **58**, 11085.

Figure(s):
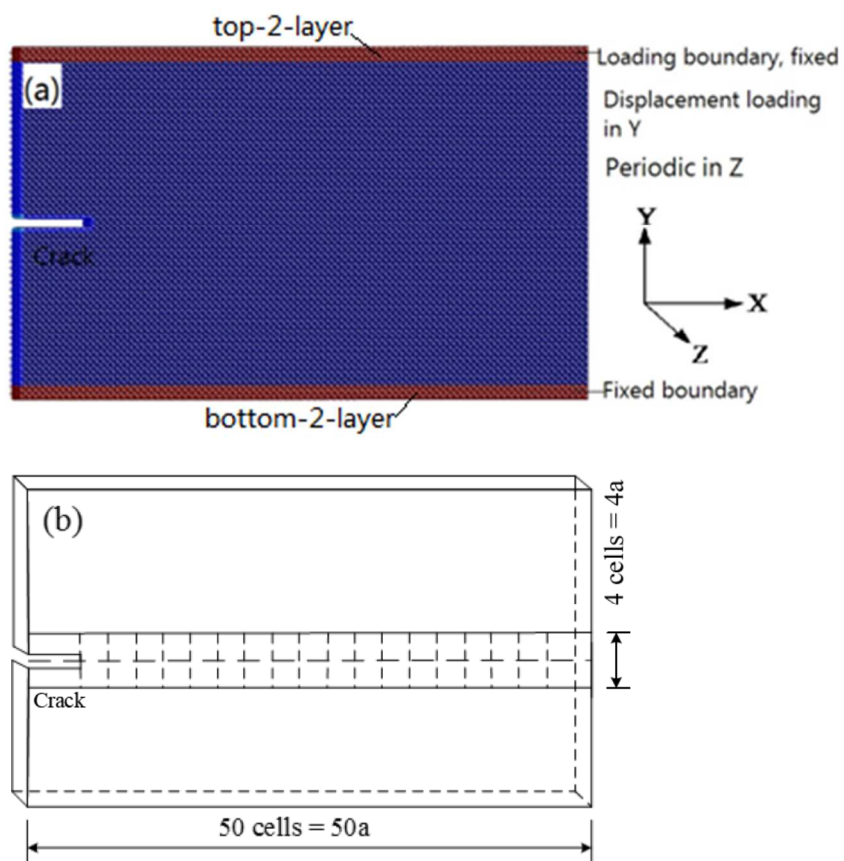
Fig.1. (a) Atomic model of an FCC single crystal nickel containing a single edge crack, (b) Schematic of region used to calculate local facture properties and obtain the cohesive behavior mechanism from MD simulation. (The width of one cell is the lattice constant of nickel).
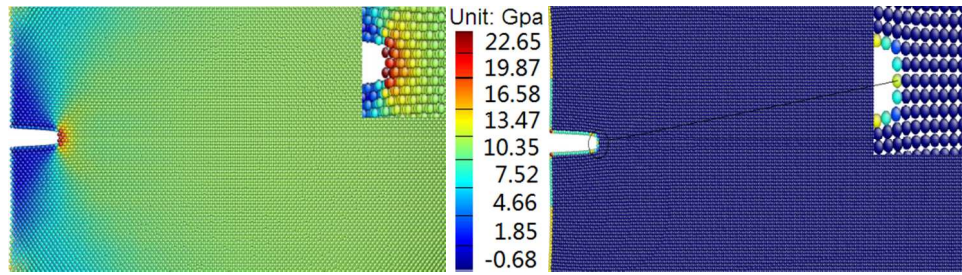
(a) t=300ps
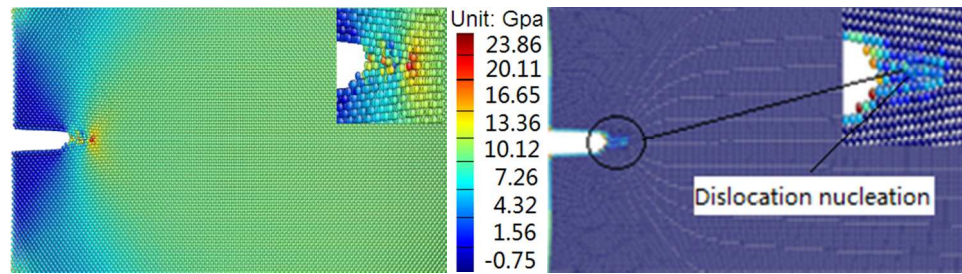
(b) t=376ps
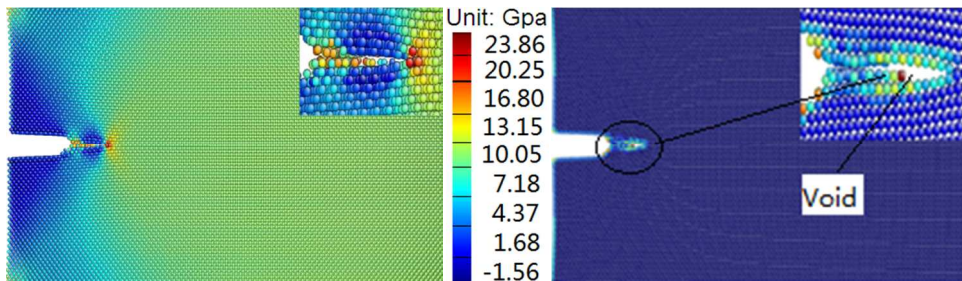
(c) t=386ps
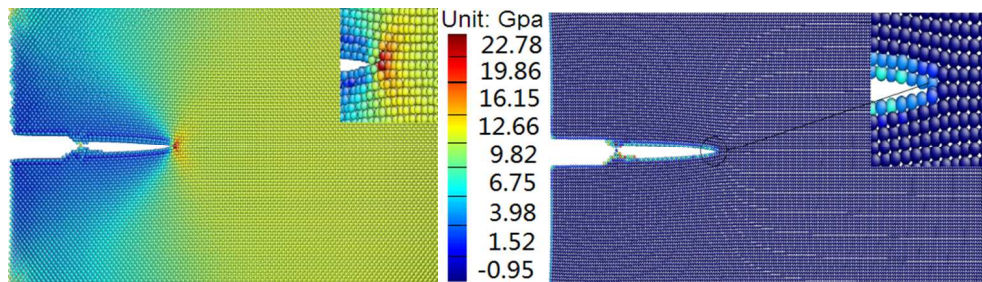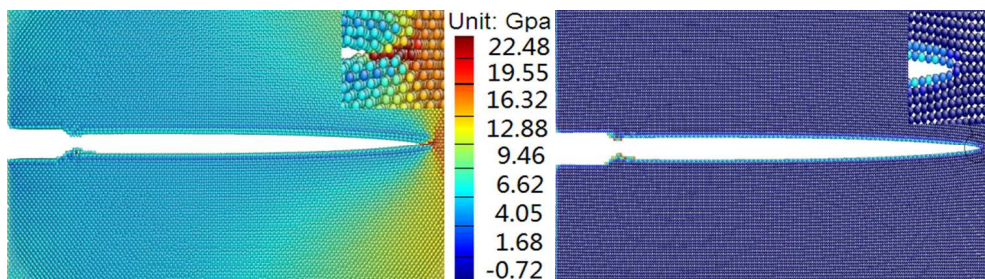
(d) t=400ps

(e) t=448ps

Fig.2. The contour plots of the atomic tensile stress field and microstructure evolution during the process of crack propagation in the X[100], Y[010], Z[001] orientation. (a) t=300ps, (b) t=376ps, (c) t=386ps, (d) t=400ps and (e) t=448ps. The insets in Fig. 2 provided a detailed view of the atomic tensile stress levels and microstructure evolutions.

Fig. 3. Atomic tensile stress as a function of the atom position along the crack path during the process of crack propagation in the X[100], Y[010], Z [001] orientation.

(a) t=150ps

(b) t=190ps
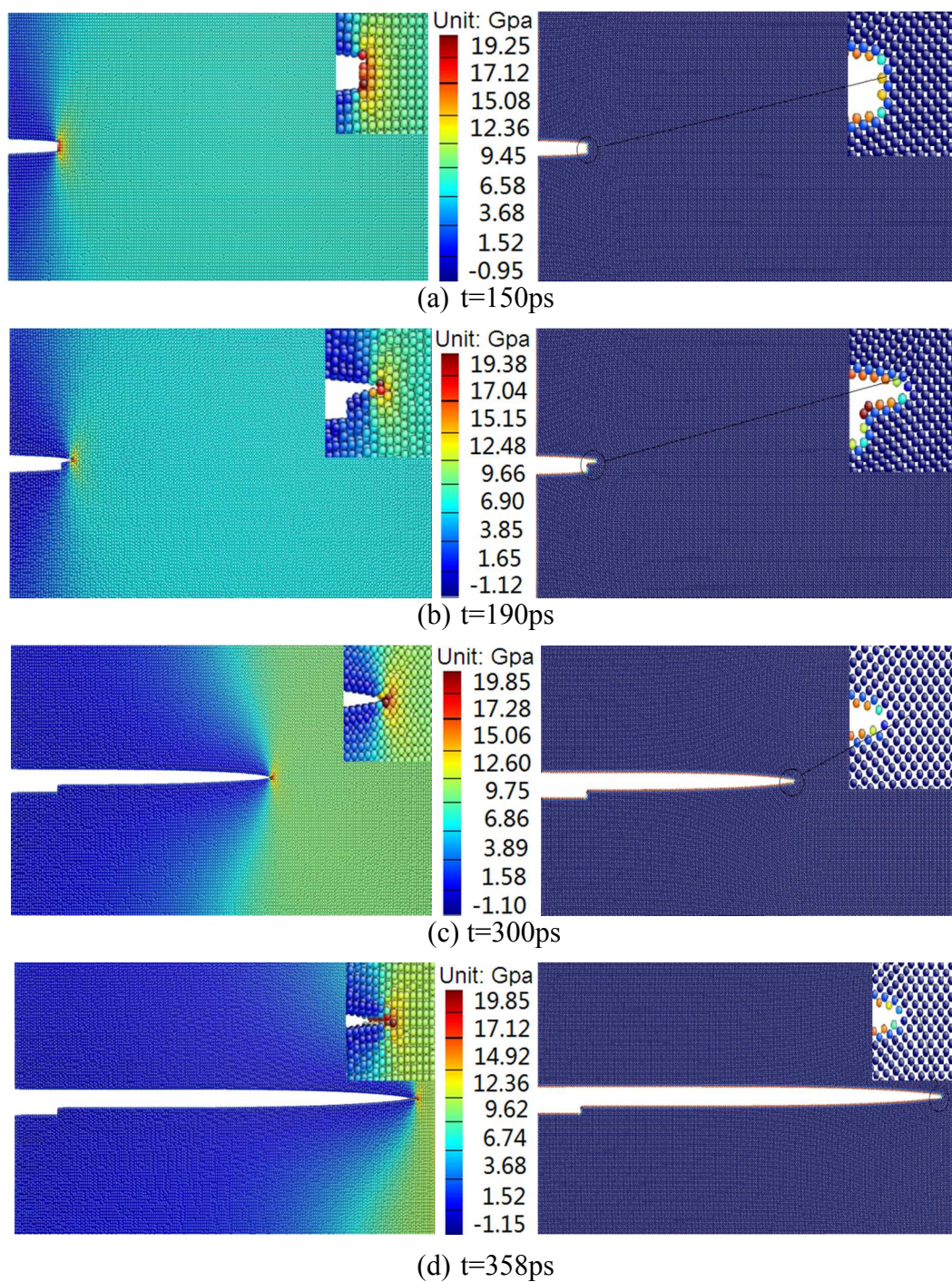
(c) t=300ps

(d) t=358ps

Fig. 4. The contour plots of the atomic tensile stress field and microstructure evolution during the process of crack propagation in the X [110], $Y[\bar{1}10]$, Z [001] orientation. (a) t=150ps, (b) t=190ps, (c) t=300ps and (d) t=358ps. The insets in Fig. 4 provided a detailed view of the atomic tensile stress levels and microstructure evolutions.
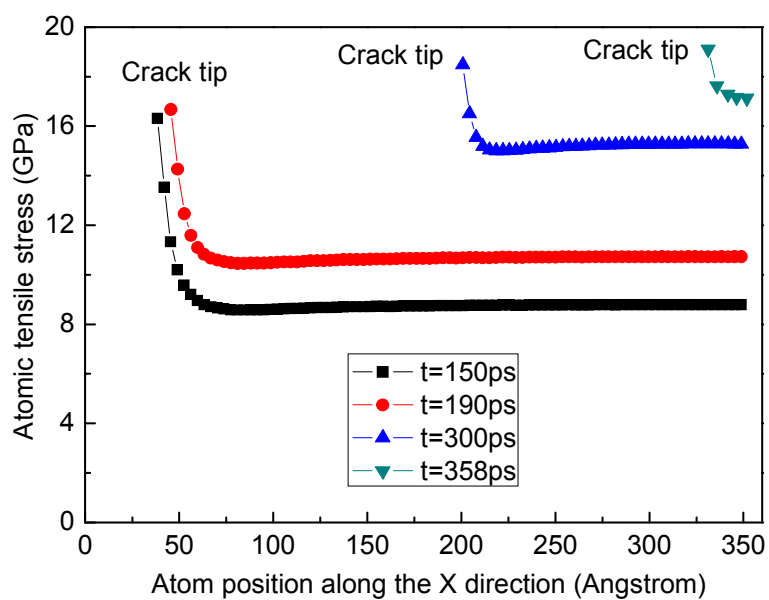
Fig.5. The atomic tensile stress as a function of atom position along the crack path during the process of crack propagation in the X [110], $Y[\bar{1}10]$, Z [001] orientation.
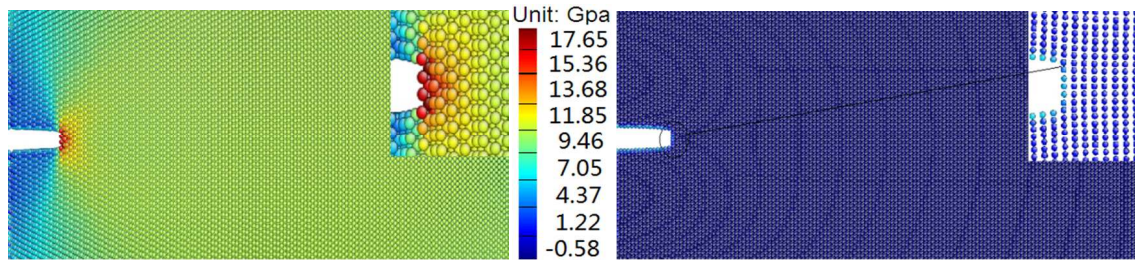
(a) t=200ps
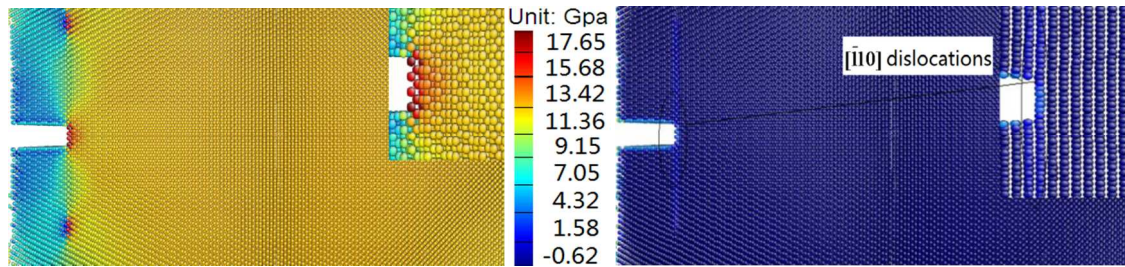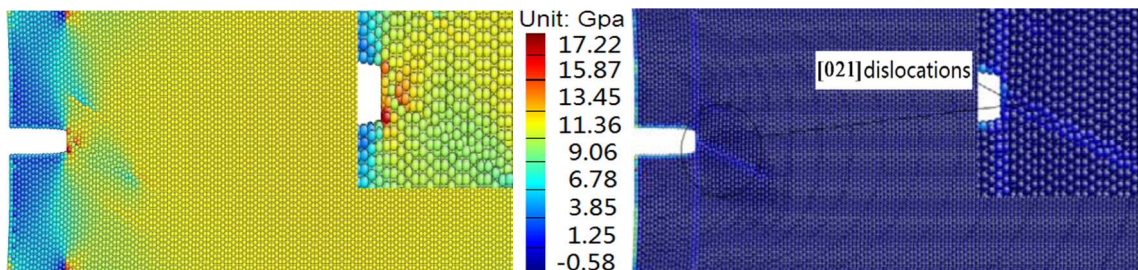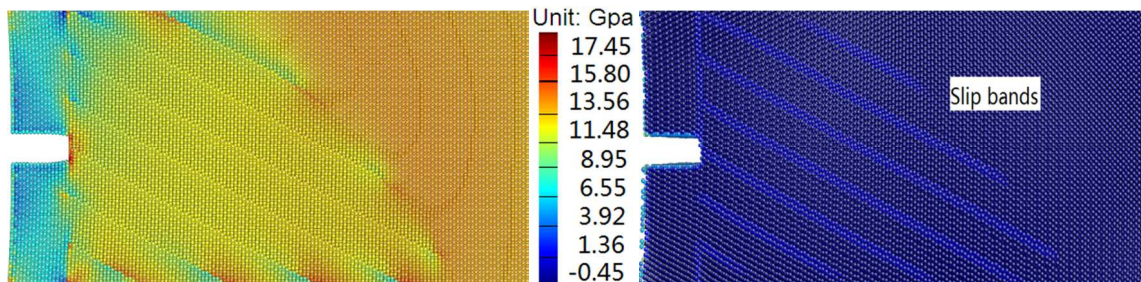
(b) t=232ps
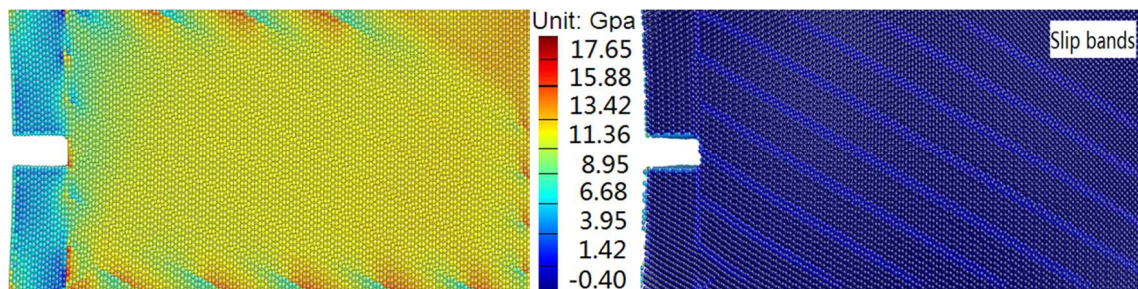
(c) t=300ps

(d) t=330ps

(e) t=350ps

Fig. 6. The contour plots of the atomic tensile stress field and microstructure evolution during the process of crack propagation in the X [111], $Y[\bar{1}10]$, $Z[\bar{1}\bar{1}2]$ orientation. (a) t=200ps, (b) t=232ps, (c) t=300ps, (d) t=330ps and (e) t=350ps. The insets in Fig. 6 provided a detailed view of the atomic tensile stress levels and microstructure evolutions during the process of crack propagation.
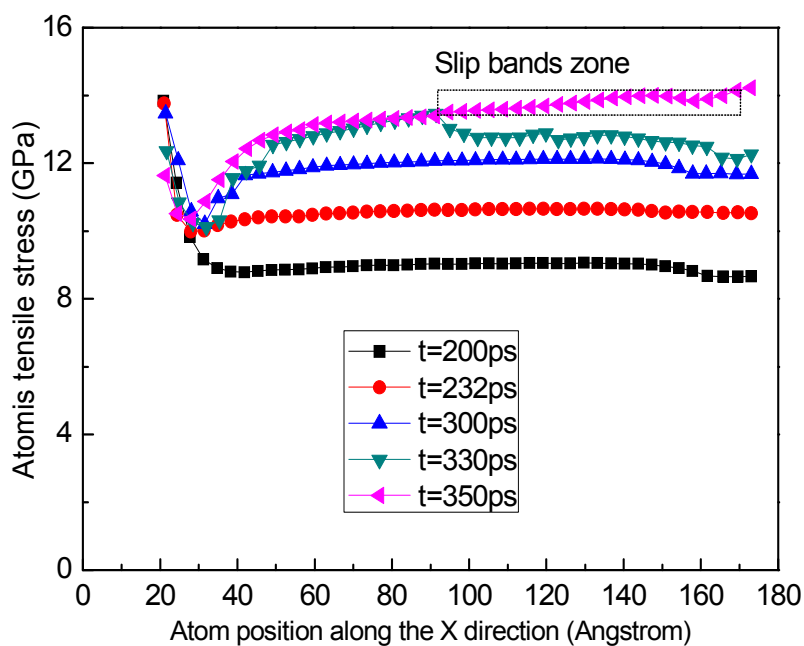
Fig.7. The atomic tensile stress as a function of atom position along the crack path during the process of crack propagation in the X [111], $Y[\bar{1}10]$, $Z[\bar{1}\bar{1}2]$ orientation.
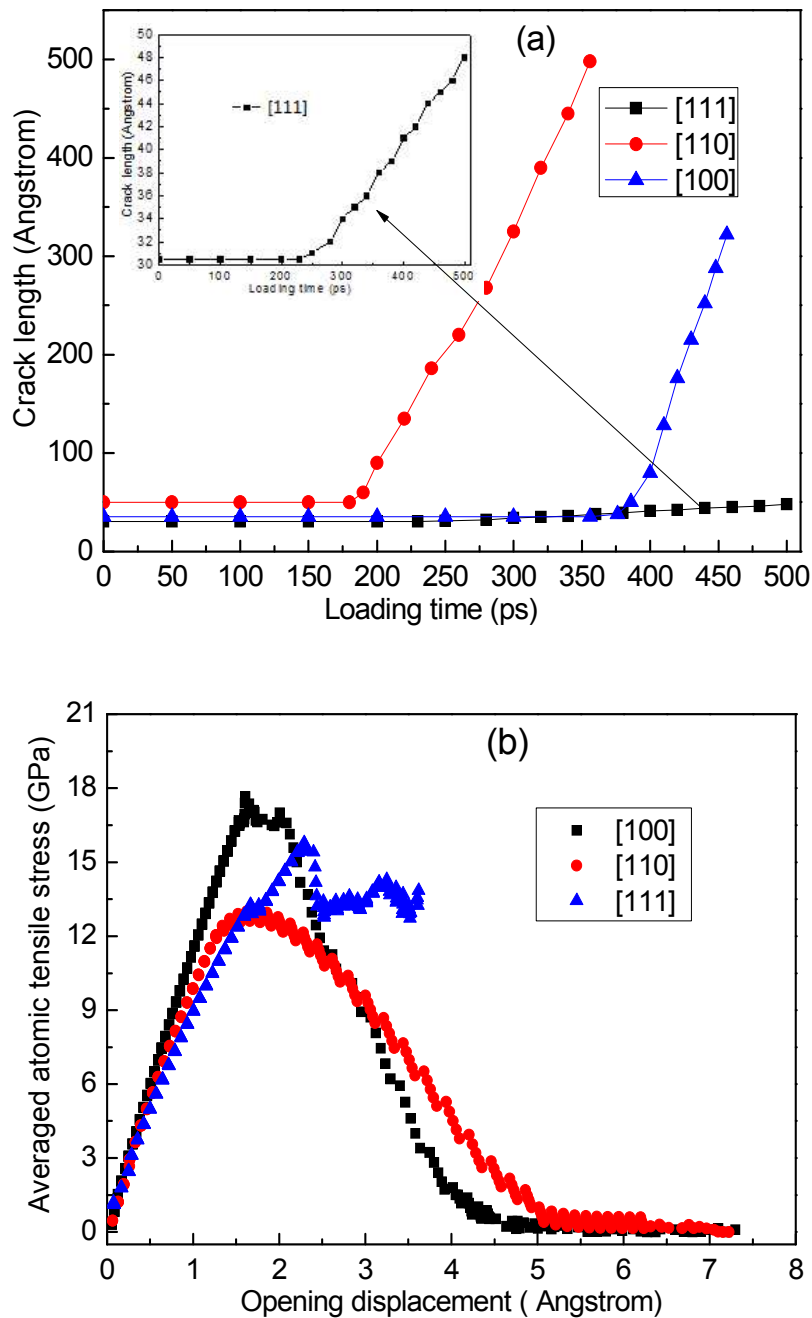
Fig. 8. Crack propagation dynamics of samples with different orentations : (a) crack growth length vs. loading time; (b) averaged atomic tensile stress vs. the opening displacement.

Table(s):

Tab.1.   Atomic configuration for the crack models with three different orientations (a = 3.52 Å is the lattice constant of nickel).

Orientation (X,Y,Z)	Model size (X,Y,Z)	Crack size (X,Y,Z)	Number of atoms
[100], [010], [001]	$100a \times 50a \times 6a$	$10a \times a \times 6a$	121428
[110], $[\bar{1}10]$, [001]	$100a \times 50a \times 4a$	$10a \times a \times 4a$	159588
[111], $[\bar{1}10]$, $[\bar{1}\bar{1}2]$	$50a \times 25a \times 6a$	$5a \times a \times 6a$	119878